Journal of Positive Sciences (JPS) eISSN: 2582-9351, https://positive-sciences.com JPS. 2025 May; 5(3): 47-63

Article info
Received on: 11.03.2025
Accepted on: 20.05.2025
Published on: 31.05.2025
doi: https://doi.org/10.52688/ASP84090

Research Article

Integrated SPA-L, Mechanical, and Antibacterial Evaluation of High-Purity Aluminum: Linking Plasma Signatures to Alloy Performance

Bilal Ahmed Hbeeb [1, *]

[1] Collage of production Engineering and metallurgical, University of Technology- Iraq, Baghdad, Iraq

[*] 70123@uotechnology.edu.iq

ABSTRACT

This paper describes a diagnostic investigation of aluminum plasma for simultaneously evaluating the spectral and mechanical characteristics of a high-purity Al alloys. A Stimulated Plasma Analysis by Laser (SPA-L) system based on a pulsed Nd:YAG laser was created to produce and study plasma in air. The Distinct Spectral Plasma Sign (DSPS) and Curve Fitting Solution revealed twelve strong analytical Al lines (AL1-AL12), which were then utilized to determine plasma parameters and elemental concentrations. The plasma temperature and electron density were determined to be t_p=7586.9°C and $\rho \approx 8.83\times10^{12}$ cm^{-3}, with a very low average relative divergence from NIST wavelengths ($\approx 1.35\times10^{-4}$), validating the diagnostics' trustworthiness. Quantitative SPA-L analysis confirmed aluminum as the primary element (~97.6 wt.%), with total petty impurity and trace additions of 2.166, 0.1899, and 0.0139 wt.%, respectively. This revealed several minor elements that were not discovered by XRF, which only recognized Al, Fe, Si, and Mg. XRD verified a single-phase FCC Al matrix. AFM revealed homogenous nanoscale surface roughness. Tensile studies on three alloy classes (X1-X3) at room temperature and 125°C revealed that minor-element composition changes had a considerable effect on yield strength, ultimate tensile strength, and strain hardening, with strength decreasing as temperature increases.
Antibacterial activity tests against Escherichia coli, Acinetobacter baumannii, Staphylococcus aureus, Staphylococcus citrus, and Streptococcus faecalis revealed inhibition zones of only 8-9 mm, equivalent to the well diameter, indicating that the treated surfaces had no significant antibacterial effect under the tested conditions. The findings reveal that SPA-L is a sensitive, fast, and basically non-destructive method for connecting plasma diagnostics, alloy chemistry, and mechanical performance in a high-purity Al alloys aluminum conductors.

KEYWORDS: A high-purity Al alloys, alloy elements, mechanical properties, assignment points properties, curve fitting solution

INTRODUCTION

Aluminum is one of the lightest engineering metals, having a strength-to-weight ratio superior to steel [1]. Aluminum represents about 8% of the Earth's crust and is distributed in the Earth's rocks in a greater percentage than all other metals. Pure aluminum is a silvery-white metal that is soft and flexible and whose weight is very light. Its specific density is 2.7 g/cm³, which is equivalent to one-third of the specific weight of steel. It is a good conductor of heat and electricity, as its conductivity is two-thirds of copper, and on the other hand, it is a low-hardness metal that does not exceed 40 HB, and its tensile strength does not exceed 90 N/mm². In recent years, aluminum and aluminum alloys have been widely used in more industries. Pure aluminum is ductile, soft, has good corrosion resistance, and has a high electrical conductivity [2-4]. Thus, in most applications and fields, aluminum is used in the form of alloys by

*Corresponding author
Bilal Ahmed Hbeeb,
Collage of production Engineering and metallurgical, University of Technology- Iraq, Baghdad, Iraq
e-mail: 70123@uotechnology.edu.iq

adding alloying elements to aluminum, and the basic elements that are added to aluminum are Cu, Mg, Mn, Si, Zn, and other elements. By adding these elements to pure aluminum, aluminum alloys are produced, which are numbered according to the Aluminum Association [5]. Each series has a unique feature, like the first series of a high-purity Al alloy, which has great electrical conductivity and is used in electrical applications [6]. By adding some alloying elements in specific proportions, the properties (physical, chemical, and mechanical) of aluminum alloy can be improved [7]. The main alloying additions, or impurities, in these alloys are Fe, Si, Mn, etc. These elements have played a major role in improving the properties of a high-purity Al alloy while controlling minor elements and other impurities [8-11]. In this regard, this research deals with the evaluation of some alloying elements in aluminum alloys used in electrical power transmission wires, which affect their important properties [12]. Alloying elements are selected based on their effects and suitability. Alloy elements can be classified into major, minor, and impure elements, but impurity elements in some alloys can be major or minor elements in other alloys [13].

The evaluation of metallic elements is a primary concern in the mining and metallurgical industries because metals play a crucial role in many important modern applications, including medical uses, smart industries, and various other applications that rely on specific metallic alloy elements. Therefore, the qualitative evaluation process is the first and most important procedure performed by metallurgical engineers. There are two types of evaluation processes: qualitative evaluation and quantitative evaluation. Therefore, choosing an appropriate mechanism for the evaluation process is important to obtain high accuracy and efficiency and at the same time be economical and inexpensive. In this work, the Stimulated Plasma Analysis by Laser method (SPA-L) was used in the process of evaluating the elements present in this selected sample (a high-purity pure aluminum alloy). In fact, this SPA-L method is essentially inexpensive and non-destructive, which makes it attractive for the analysis of many important and complex samples [14]. This is due to some basic characteristics of its technology. It is worth noting that there are many lasers used in SPA-L technology, but that the laser (Nd-YAG) is widely used because this provides the highest energy density [15, 16]. In brief, SPA-L is a type of atomic emission spectroscopy in which a pulsed Nd-YAG laser is used to strike the sample surface with a high enough energy density to generate a plasma on that surface, and then the characteristic emission points occur for the presented elements in the sample. The generated plasma represents the diagnostic identity of all the elements composing this target sample, to give unique analytical points, which is called a fingerprint [17, 18].

In this paper, a diagnostic study was conducted on the plasma properties to determine and know the features of the peak assignments and analytic points. This study can be used to collect results and information that can be exploited in the process of analyzing and evaluating problems, failures, and errors likely to occur in the future due to the presence of these minor and impure elements in the alloy. In addition to reviewing and evaluating the efficiency and work of this alloy during work. additions, this study is to compare two studies, XRF and SPA-L, to diagnose the aluminum plasma accumulated on the surface of the sample, as this plasma represents all the important elements of the components of this sample. On the other hand, accurate quantitative qualitative determination is applied for all important major, minor, and impure alloying elements that are difficult to capture and examine through other traditional techniques; this will help in studying the effect of these elements on the mechanical properties of the alloys, which will have a significant impact on efficiency and accuracy in making this alloy sample practical for applications. Therefore, this study aims to integrate SPA-L diagnostics with mechanical and antibacterial evaluations of high-purity aluminum in order to link plasma signatures to alloy performance. The work focuses on diagnosing and assessing elemental composition, alloy concentrations, and tensile behavior in a selected 1xxx-series aluminum alloy. The influence of minor metallic constituents on mechanical properties was thoroughly investigated. Based on the obtained data, stress–strain curves were generated, and key mechanical parameters—yield strength (YS), ultimate tensile strength (UTS), and elongation to failure—were determined. Accordingly, the specimens were analyzed using SPA-L, XRF, tensile testing, XRD, AFM, and antibacterial activity measurements at ambient temperature.

EXPERIMENTAL WORK

An experimental array was designed using the pulsed/laser system with a pulse time of 7 nm and a wavelength of 1064 nm for the aluminum alloy sample used in electrical power transmission. These parameters were used to excite and generate the aluminum macro-plasma. A single shot of 100 mJ laser energy was directed at the surface of an aluminum alloy sample with a spot breadth of 1 mm by a lens with a focal length of 100 mm. As a result of applying

*Corresponding author
Bilal Ahmed Hbeeb,
Collage of production Engineering and metallurgical, University of Technology- Iraq, Baghdad, Iraq
e-mail: 70123@uotechnology.edu.iq

these parameters, the peak power of the laser beam pulse was 14.28 MW, and the maximum power density was 1.82×10^{9} watts cm^{-2}. The released optical plasma emission of the aluminum tested is collected by a lens with a focal length of 15 mm and directed onto an optical fiber cable, which delivers plasma light to the entry aperture of the analyzer (CCS-100 model), with a grating (1200 lines/mm) and a slit distance of 20 µm. It scatters light depending on its wavelength and then reflects it using mirrors. Then it focuses on detecting optical signals, converting them to digital, and then transporting them by sending a digital signal to the application that displays us the spectral points of the sample and then analyzes it.

In this work, an aluminum alloy sample used in electrical power transmission was analyzed according to order (1.4% iron (Fe), 0.558% silicon (S), 0.042% magnesium (Mg), and the remaining aluminum (Al)) by preliminary XRF examination. The sample was prepared by cutting the aluminum alloy wire into a small disk with a diameter of 1 mm and a height of 1 mm and preparing it for examination using 100, 250, and 500 smoothing paper.

It is worth noting that XRF is unable to analyze all elements with atomic numbers between 12 and more than 92. In addition to some limitations that make this technique unable to evaluate all metals with high or varying accuracy, this is one of the problems that can be overcome with SPA-L technology, and this is one of the reasons that made us choose this technology in this work. This technology is considered one of the most powerful technologies and competes with other inspection technologies, for example, X-ray fluorescence (XRF) technology used in metal inspection. The experimental arrangement of the SPA-L setup built in our laboratory is shown in the Fig. 1 and the following parts: Workspaces (for the quality evaluation), Pulsed/Laser Beam (to produce the macro-plasma), Lenses (to focus the laser beam), Optical Cable (to transition the emission spectral point), Spectrum Analyzer (to analyze the emission spectral point), and Computer (to control the data by program).

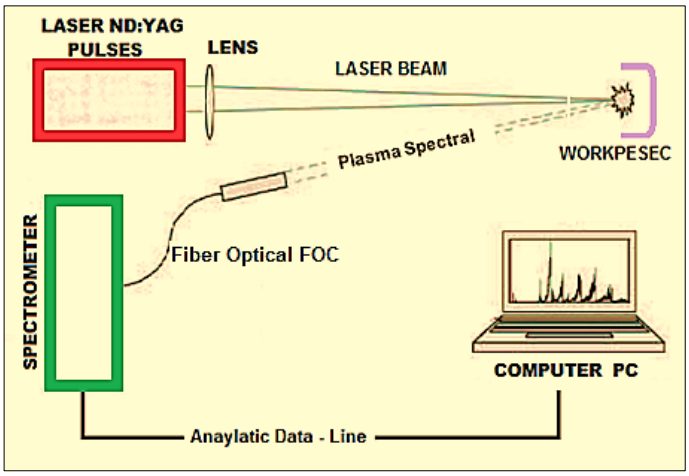

Fig. 1 The A set-up of experimental

To evaluate the tensile properties behavior of each selected a high-purity Al alloy specimen, the tensile test process was conducted at 25°C temperatures. For the X1, X2, and X3 classes, the yield strength (YS) and ultimate tensile strength (UTS) were considered. Specimens were fabricated from the section with standard dimensions, based on the ASTM standard, where the diameters were 12 mm and the gauge length was 240 mm for the rods. The rods were machined using a computer numerical control (CNC) cutting machine.

For the tensile testing machine, the elongation rate was set at 1 mm/min, with a preload of 200 N. A computer program was used to monitor deformation behavior and calculate strain values. Each tested specimen generated a specific stress–strain curve, which was analyzed to evaluate tensile properties and deformation behavior using load-deformation (KN-mm) and stress–strain (Mpa) curve methods.

All experiments were conducted under constant and controlled environmental conditions. A Shimadzu MXF2400 multichannel X-ray fluorescence system and a MICRO-computer-controlled universal testing machine (WDW-200E) were utilized. The XRF results were subsequently compared with the corresponding SPA-L data, in addition to complementary XRD and AFM analyses.

*Corresponding author
Bilal Ahmed Hbeeb,
Collage of production Engineering and metallurgical, University of Technology- Iraq, Baghdad, Iraq
e-mail: 70123@uotechnology.edu.iq

ANTIBACTERIAL ACTIVITY

Agar Diffusion Method (ADM) is one of the conventional method used for screening anti-bacterial activity of chemical compounds, extracts, coating and nanoparticles. In this procedure, the biosurfactant diffuses through a solid agar matrix previously inoculated with a standardized suspension of microbial organisms. The substance diffuses from the point of application and it inhibits growth in a concentration dependent way, leading to a zone free of bacteria on all sides of the area applied.

In the ADM protocol culture media are scheduled (usually MH agar for bacteria) and sterilized before pouring out in Petri plates. The agar is allowed to set and its surface in the dish or plate is evenly spread by the test microorganism, via spreading onto that standardized inoculum (e.g., 1.5×10^8 CFU/mL using a 0.5 McFarland turbidity standard). Wells can then be punched out on the agar (well diffusion technique), or sterile discs saturated with the test material spread directly onto the surface of the medium (disc diffusion technique). Plates are incubated at standard conditions usually 37°C for 24 h for usual bacterial strains..

Following incubation, zones of inhibition—clear regions around the wells or discs—are measured to quantify antimicrobial potency. Larger zones indicate greater antibacterial activity due to more effective diffusion and microbial growth inhibition. The ADM is valued for its simplicity, reproducibility, and suitability for preliminary screening of antimicrobial properties across a variety of microorganisms.

RESULTS AND DISCUSSION

Metal alloys are distinguished from other materials by some distinctive properties, such as physical, mechanical, chemical, biological and spectral properties. In this effort, a diagnostic study was conducted to estimate the important parameters of spectral properties, mechanical and antibacterial properties, which was highlighted in this work for describing and giving information about estimating the alloying elements' concentration, which is determined. These alloying elements affect the mechanical and antibacterial properties of metal alloys used in specific applications, such as 1xxx-aluminum alloy.

ESTIMATE OF THE ANALYTICAL-POINTS PROPERTIES

Through the laser interaction with the selected aluminum alloy, the Distinctive Spectral Plasma Signature (DSPS) of the aluminum plasma (macro-plasma) at the region from 200 to 800 nm was produced. It was recorded by the wavelength at 1064 nm of laser (Nd-YAG), with the density of the laser power at 1.82×109 W/cm². The spectral plot was acquired using single laser shot data under the best conditions; it was chosen after several attempts, and it was revealed in Fig. 2. The emitted spectral signature consists of individual neutral and ionized spectral points of the foremost element and other petty, impure elements present in the sample; it shows the intensity peaks of the detected unique wavelengths (G̈) of all the observed spectral points of the aluminum plasma formed, which are unique spectra.

The Assignment-Points AP that represent the spectral points with the highest intensity values for the neutral and individual ionized transitions of all the petty, impure, and trace elements, which form the spectral map of the plasma formed, as shown in Fig. 3.

In addition to the analytical points representing the spectral points with the highest intensity value for the natural and ionic transformations of the foremost element (aluminum metal), in our work through this research, the analytical points of aluminum metal are (AL1, AL2, AL3,…AL12) as shown in Fig. 4.

where :

The Distinctive Spectral Plasma Sign **DSPS =A**ssignment Point **(A_P) + A**nalytic **P**oint (**AL_{1-12}**) (1)

[Petty - Trace Elements] [Foremost Metal]

*Corresponding author
Bilal Ahmed Hbeeb,
Collage of production Engineering and metallurgical, University of Technology- Iraq, Baghdad, Iraq
e-mail: 70123@uotechnology.edu.iq

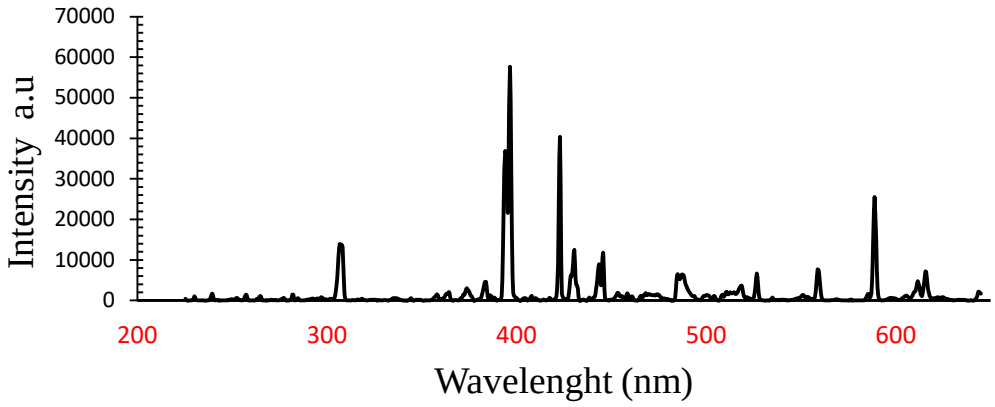

Fig. 2. Distinct spectral sign of the Aluminum-plasma released from through the interaction of laser with the Aluminum sample at the region from (200-800) nm

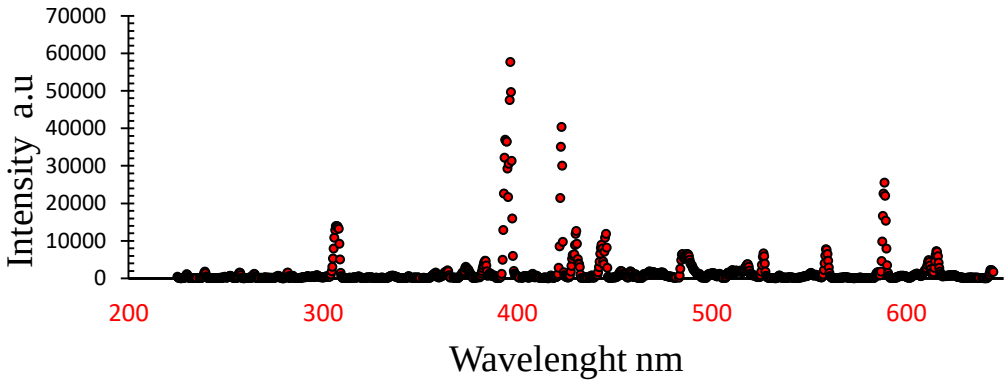

Fig. 3. All peak assignment points (A_P) in the spectral plot of all Aluminum-plasma components of the selected sample in the region from (200-800) nm

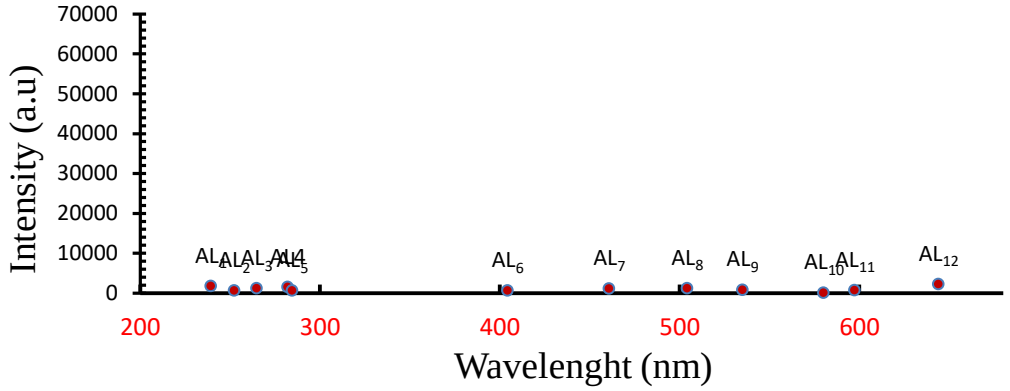

Fig. 4. Strong analytical points in the spectral plot of aluminum-plasma content at the region from (200-800) nm.

To calculate the relative divergence percentage with NIST-ASD (standards database), the values of the actually emitted, practically captured unique wavelengths ($\ddot{G}\ddot{O}$) of the plasma were obtained from the ND:YAG laser stimulation process. Using the numerical analysis solutions and through Eq. 4. The relative and absolute error of the matching process with the Standards and Technology Atomic Spectra Database [standard wavelengths Ws] was calculated, and the approximate values of Detection and Intersection were found for all the peak assignments (I:Y axis) and wavelengths ($\ddot{G}\ddot{O}$:X axis), which represent all the selected metallic elements, as shown in the relative and absolute divergence in front of each analytic point in Table 1.

$$\text{Divergence Degree} = \text{Stander Wavelength}\ (\ddot{W}) - \text{Detected Wavelength}(\bar{\ddot{W}}) \quad (2)$$

*Corresponding author
Bilal Ahmed Hbeeb,
Collage of production Engineering and metallurgical, University of Technology- Iraq, Baghdad, Iraq
e-mail: 70123@uotechnology.edu.iq

$$\text{Absolute Divergence } \theta = \frac{(\ddot{W}) - (\bar{\ddot{W}})}{(\ddot{W})} \quad (3)$$

$$\text{Relative Divergence R.D \%} = [\text{ Absolute Divergence } \theta * \% \ 100 \ ] \quad (4)$$

where the detection process represents the process of capturing the intensity of the emitted wavelengths ($\bar{\ddot{G}}$) from the laser-stimulated plasma through a spectrometer within the range of 200-800 nanometers. Taking into account the creation of all appropriate practical conditions is to conduct and complete the capture process.

As for the intersection process, it represents the process of matching and comparing the wavelengths emitted ($\bar{\ddot{G}}$) and practically detected from the plasma (unique wavelength) with the standard wavelengths ($\ddot{W}$) to find all analytic points for aluminum metal present in the spectral signature detected for the plasma.

In our experimental conditions, as shown in Fig. 4, all spectral points in the detected spectral plot that represent the analytic points [AL1 ... AL12] of unique wavelengths $\bar{\ddot{G}}$ at region (200-800) nm, which observe major aluminum content of the sample used.

A specific number of wavelengths were selected from the spectral plot (237.839–663.121 nm) as an illustrated example to illustrate the degree of correspondence between the standard wavelengths ($\ddot{W}$) obtained based on NIST-ASD and some references [19, 20, 21] and the wavelengths emitted ($\bar{\ddot{G}}$) and practically captured of the formed plasma in this work, as shown in Table 1.

Table 1. The divergence amount with NIST standard wavelengths ($\ddot{W}$) for the values of the practically captured wavelengths ($\bar{\ddot{G}}$) and the relative divergence (ϵ%) of the capture process

$\ddot{W}$ (nm)	$\bar{\ddot{G}}$ (nm)	Analytic point	Intensity (a.u)	Divergence Degree	Absolute Divergence θ	Relative Divergence R.D %
237.8395	237.8391	AL $_1$	1690	0.0004	1.68E-06	1.68E-04
256.7983	256.798	AL $_2$	617.1	0.0003	1.17E-06	1.17E-04
265.2475	265.2478	AL 3	1118.2	0.0003	1.13E-06	1.13E-04
281.6185	281.619	AL $_4$	1443.5	0.0005	1.78E-06	1.78E-04
305.0072	305.0074	AL $_5$	574.55	0.0002	6.56E-07	6.56E-05
396.152	396.152	AL $_6$	562.16	0	0.00E+00	0.00E+00
474.0265	474.0268	AL $_7$	1040.4	0.0003	6.33E-07	6.33E-05
510.752	510.756	AL $_8$	1163.9	0.004	7.83E-06	7.83E-04
510.7943	510.7944	AL $_9$	716.39	1E-04	1.96E-07	1.96E-05
555.7063	555.7065	AL $_{10}$	47.321	0.0002	3.60E-07	3.60E-05
555.7948	555.7946	AL $_{11}$	658.21	0.0002	3.60E-07	3.60E-05
663.1218	663.1221	AL $_{12}$	2171.9	0.0003	4.52E-07	4.52E-05
…		…		**0.000567**	**1.35E-06**	**Avg. : 1.35E-04**

The strong analytic points of aluminum metal (foremost) appear under the above spectral map of plasma, from by this Analytic Points AL (Al1 – Al12) for the selected sample can determine the atomic constants used to evaluate the temperature and densities of the aluminum-plasma, where the points are shown in Fig. 4 .

Table 2 illustrates the atomic spectroscopy properties that were used to determine the plasma factors, where the temperature of plasma can be estimated through the following Eq. 5

$$[\text{Ln } (I/ P_T * S_w) - \text{Ln } (C_e * F / P_F)] * k * t_p = - Б \quad (5)$$

where I is the intensity value of spectral points, PT is the probability of transitioning from one energy level to another, Sw represents the statistical weight of the upper level, tP expresses the temperature of the plasma, PF is the partition function, Ce is the concentration of elements, Б is the excited upper-level energy, El is the excited lower-level energy, and k = (0.695) is the constant.

*Corresponding author
Bilal Ahmed Hbeeb,
Collage of production Engineering and metallurgical, University of Technology- Iraq, Baghdad, Iraq
e-mail: 70123@uotechnology.edu.iq

The result of t_P is the slope of a straight line for the average analytical points, which is expressed as ($-1/k \times t_P$). Where the equation of the straight line is $Y = A_o + A1\ X$. When Eq. 6 matches the general straight line equation, it becomes clear that:

$$[Ln\ (I / P_T \times S_w)] = [Ln\ (C_e .F / P_F)] - [1/ k \times t_P] \times Б \quad (6)$$

$$Y = A_o + A_1\ X \quad (7)$$

$$Y = Ln\ (I/ P_T \times S_w),\ A_o = Ln\ (C_e .F / P_F),\ A_1 = -1/k_* t_P \text{ and } X = Б \quad (8)$$

where the slope of average analytic points is expressed as follows: $Ş = A_1 = (-1/k \times t_P)$ (9)

Table. 2. The spectroscopy properties of the aluminum-analytical points emitted from aluminum plasma according to NIST standard selection

No.	Wavelength (nm)	Intensity (a.u)	Analytical Points AL I	P_T	S_w	E_i	Б
1	237.8395	1690	AL $_1$	9.34E+06	2	0.013894	5.22524
2	256.7983	617.1	AL $_2$	2.20E+07	4	0	4.826631
3	265.2475	1118.2	AL $_3$	1.34E+07	2	0	4.672892
4	281.6185	1443.5	AL $_4$	3.93E+08	1	7.420705	11.821968
5	305.0072	574.55	AL $_5$	3.21E+07	6	3.603844	7.667622
6	396.152	562.16	AL $_6$	1.01E+08	2	0.013894	3.142721
7	474.0265	1040.4	AL $_7$	8.71E+04	4	3.142721	5.757544
8	510.752	1163.9	AL $_8$	2.57E+05	4	3.142721	5.569528
9	510.7943	716.39	AL $_9$	2.57E+05	2	3.142721	5.569327
10	555.7063	47.321	AL $_{10}$	4.19E+05	4	3.142721	5.373212
11	555.7948	658.21	AL $_{11}$	4.20E+05	2	3.142721	5.372857
12	663.1218	2171.9	AL $_{12}$	5.04E+05	6	4.021481	5.89067

Table. 3 shows the six distinct analytical points specific for AL I (AL5, AL7, AL8, AL9, AL11, and AL12) (305.0072, 474.0265, 510.752, 510.7943, 555.7948, 663.1218 nm) in one shot of the laser pulse, which produces the best approximate line rate, and depending on numerical analysis and using the Curve Fitting Solution C.F.S., which is based on the extracted and prepared data in Table 3. Through the two equations. 10 and 13 for this method, the values of the constant Ao and A1 were extracted and replaced with the general straight line equation to find the slope value, as shown in the following equations

$$\Sigma\ Y_1 = N\ A_o + A_1\ \Sigma\ X_1 \quad (10)$$
$$-25.2 = 3 \times A_o + A1 \times 18.78 \quad (11)$$
$$\Sigma\ Y2 = N\ A_o + A1\ \Sigma \quad (12)$$
$$-20.79 = 3A_o + A1 \times 16.59 \quad (13)$$

After finding and replacing the values of the extracted constants (A_o and A_1) with the general straight line equation, the slope value is obtained for the specified analytical points. After compensating the slope value with the above equations, it will produce an average temperature of 7586.94°C for the aluminum plasma formed.

$$Y = 4.18 - 2.01\ X \quad (14)$$

where A1 = 2.01 and the slope (Ş) is expressed as follows:

$$A1 = Ş = (-1/k \times t_P),\ t_P\ (e.v) = \frac{1}{(k\ .Ş)},\ t_P\ (kelvin) = t_P\ (e.v) \times 1.1 \times 10^4 \quad (15)$$

$$t_P\ (^oC) = t_P\ (kelvin) - 273 \quad (16)$$

*Corresponding author
Bilal Ahmed Hbeeb,
Collage of production Engineering and metallurgical, University of Technology- Iraq, Baghdad, Iraq
e-mail: 70123@uotechnology.edu.iq

Table 3. The six strong analytical points for calculating constants by Curve Fitting Solution (C.F.S.)

NO.	Wavelength G̈ [nm]	Intensity I (a.u.)	Analytic points $AL_{(1-12)}$	$X = E_u$	$Y = Ln(I/P_T . S_w)$
1	305.0072	574.55	Al I	7.667622	-12.7238
2	474.0265	1040.4	Al I	5.757544	-5.81421
3	510.752	1163.9	Al I	5.569528	-6.78476
N=3				ΣX_1: 18.99469	ΣY_1:-25.32275
4	510.7943	716.39	Al I	5.569327	-6.57459
5	555.7948	658.21	Al I	5.372857	-7.15116
6	663.1218	2171.9	Al I	5.89067	-7.23893
N=3				ΣX_2: 16.83285	ΣY_2:-20.9646744

In experimental conditions, the main ionization process is produced by high laser energy collision excitation with material electrons, whereby the McWhirter criterion, which can be calculated by Eq. 17 below, the minimum plasma density for local thermodynamic equilibrium (L.T.E.) can be expressed [22, 23].

$$(\rho)^e = 1.6 \times 10^{12} \times \sqrt[2]{t_P}\ (E_i - Б)^3 \quad (17)$$

where ΔEu (eV) is the highest energy transition carried by the state, and t_P (eV) is the plasma temperature, which is achieved during the first stages of the plasma's life. However, for any ρ, it is possible to calculate it through Eq. 17. Fig. 5 shows the plasma density, showing the density of analytical points and identifying the analytical point with the ultimate density for Al1 at 237.839 nm; it is 2.014×10^{14} cm^{-3}.

*Corresponding author
Bilal Ahmed Hbeeb,
Collage of production Engineering and metallurgical, University of Technology- Iraq, Baghdad, Iraq
e-mail: 70123@uotechnology.edu.iq

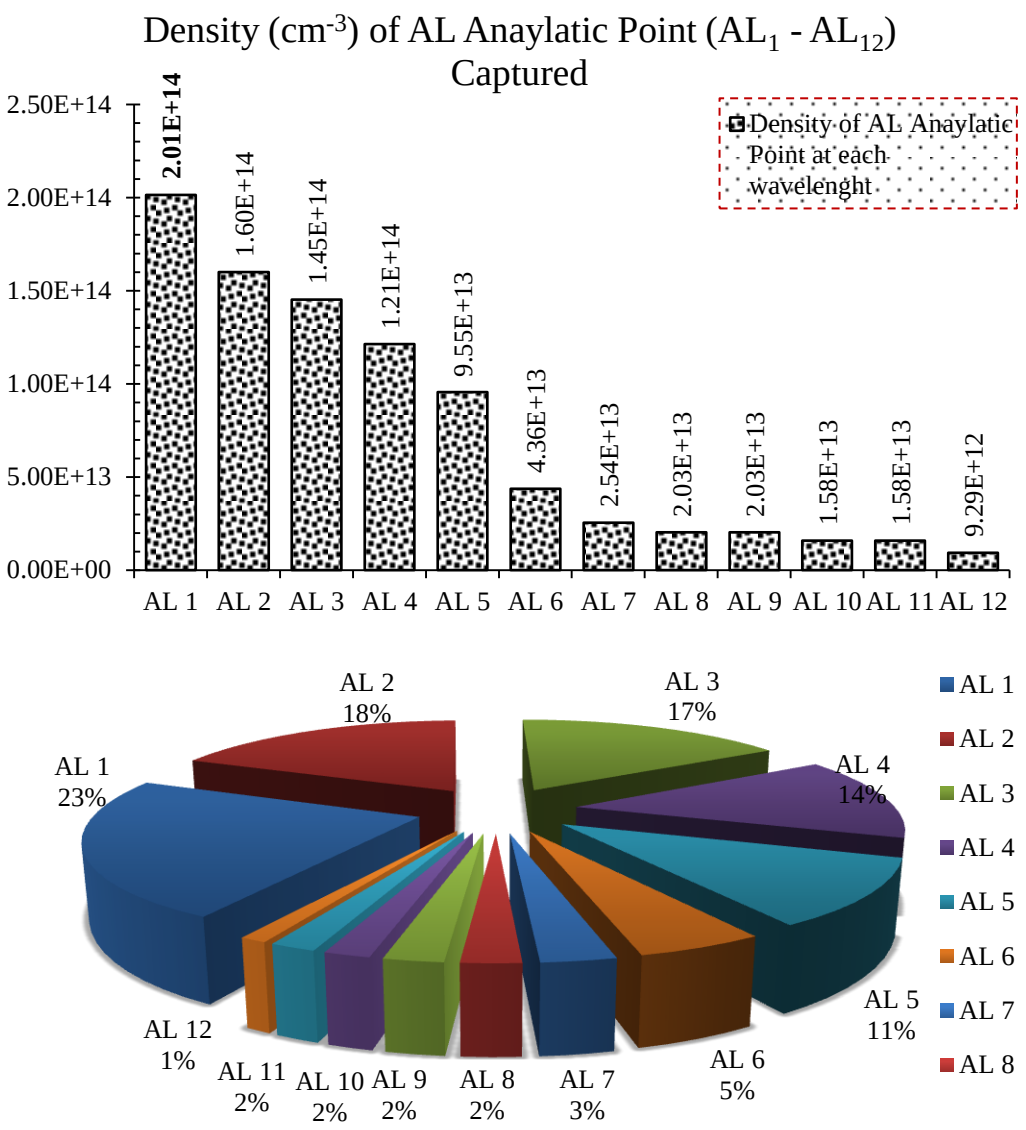

Fig. 5. The density of analytical points for AL-plasma formed

PERCENTAGE CALCULATION FOR ANALYTICAL AND ASSIGNMENT ELEMENTS

The numerical analysis Module - Curve Fitting Solution C.F.S can be used for quantitative analysis of constituent elements in aluminum-alloy samples. The mass abundance of any element in the released plasma can be determined by estimating the important parameters of plasma released through interaction of laser with aluminum-alloy samples and by evaluating the sum of the specification and analytical points of the aluminum-alloy sample, according to the following equations

$$(P_F)^T = \sum(S_w)^e \times e^{-Б/t_P} \quad (18)$$

$$(C_e) = \frac{(P_F)^T \times (e)^{\frac{-E\,ion}{t_P}}}{F} \quad (19)$$

$$Mass\ Abundance = C_e \times A.W \quad (20)$$

$$Percentage\ of\ Element\ Conceteration\ (Con.\ \%)^e = \frac{\sum(C_e\ .\ A\ .\ W)^e}{\sum(C_e\ .\ A\ .\ W)^T} \quad (21)$$

*Corresponding author
Bilal Ahmed Hbeeb,
Collage of production Engineering and metallurgical, University of Technology- Iraq, Baghdad, Iraq
e-mail: 70123@uotechnology.edu.iq

where PF is the partition function for each element analytic point, (PF)T is the sum of the partition function for all element analytic points, (Sw)e represents the statistical weight of each element analytic point, and (Ce × ACe × A × W)e is the concentration for each element. (Ce × A . W) T is the sum of the concentration for all elements in the plasma spectral map (mass abundance %); e is the percentage concentration for each element presented in the plasma; and the Atomic Weight (AW) and ion energy Eion are constant and specific to each analytic point for aluminum metal, as shown in Table 4. The concentration percentage of all different elements presented in the aluminum alloy using the SPA-L technique is summarized in Table 5. In addition to estimating the ultimate lower concentration percentage for the captured AL analysis points, distinct for each wavelength as shown in Fig. 6.

Table 4. The partition function for each aluminum analytic point and the sum of the partition function for all Al-analytic points presented in the aluminum alloy

No.	Analytic point	G̈ nm	S_W	Б	$(P_F)^T$
1	AL 1	237.8395	2	5.22524	0.002704823
2	AL 2	256.7983	4	4.826631	0.008954123
3	AL 3	265.2475	2	4.672892	0.005437543
4	AL 4	281.6185	1	11.821968	3.23005E-07
5	AL 5	305.0072	6	7.667622	0.000370069
6	AL 6	396.152	2	3.142721	0.037630085
7	AL 7	474.0265	4	5.757544	0.002760006
8	AL 8	510.752	4	5.569528	0.003500574
9	AL 9	510.7943	2	5.569327	0.001750732
10	AL 10	555.7063	4	5.373212	0.004486685
11	AL 11	555.7948	2	5.372857	0.00224435
12	AL 12	663.1218	6	5.89067	0.00349872
					Σ $(P_F)^T$: 0.073338032

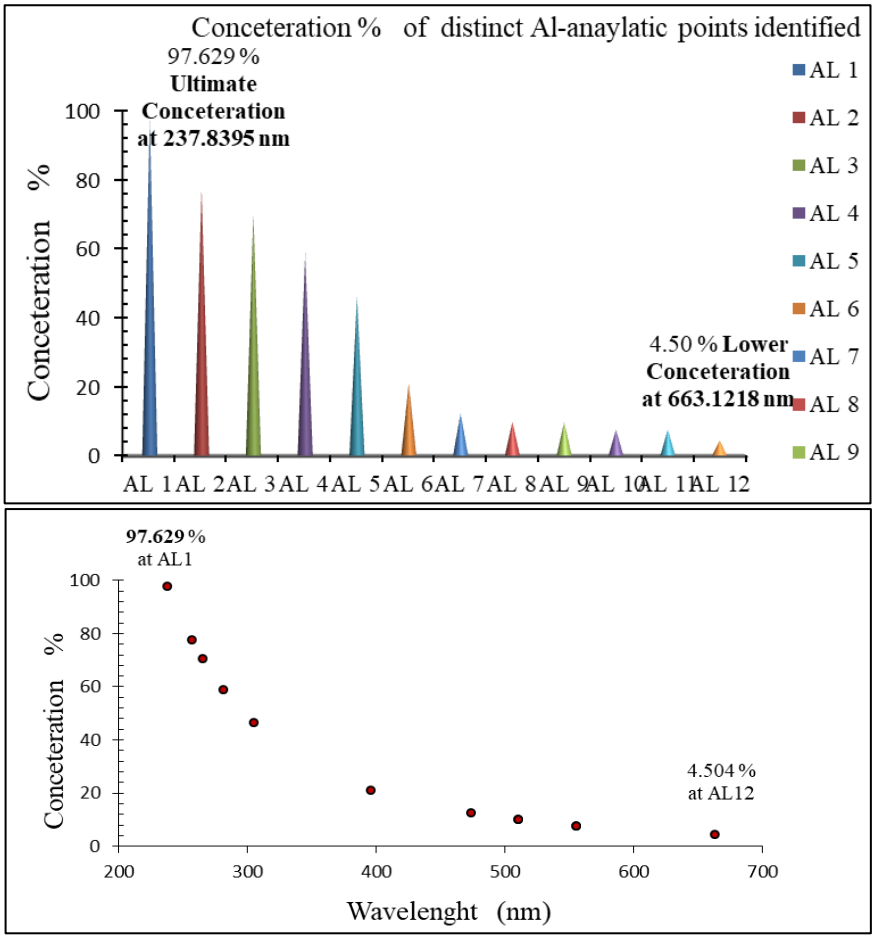

Fig. 6. The Ultimate—Lower concentration obtained for the captured AL analysis points for each wavelength

*Corresponding author
Bilal Ahmed Hbeeb,
Collage of production Engineering and metallurgical, University of Technology- Iraq, Baghdad, Iraq
e-mail: 70123@uotechnology.edu.iq

Table 5 shows that SPA-L and XRF tests were used to characterize the elements presented in the sample. Using the SPA method developed in the conditions of our practical experience, the number of metals that were captured from the examined sample was greater, as it included the foremost element, which had a concentration of approximately 97%; the petty elements, 2%; the impurity elements, 0.1%; and trace elements, 0.01%, as shown in Table 5.

As for using the XRF method, the number of metals that were captured from the examined sample was only four. The results obtained showed that there is a significant difference in the ability to detect the number of these elements through the use of the two techniques.

This is due to the dependence on the sensitivity of the reaction and the relationship between the elements to be tested (physical and chemical properties) and the testing technique used (degree of sensitivity of each technique), which varies from one element to another. In addition, the prior preparation and provision procedures of the sample before the examination process using the XRF method and other traditional methods are required and necessary, as this process depends on the skill of the person used, which varies from one person to another, as it affects the accuracy of the results of the examination process. In addition to some limitations that make XRF technology unable to detect all metals with high or varying accuracy. However, when using the SPA-L technique, the prior preparation procedures of the sample before the examination process are not required; this is an inexpensive and essentially non-destructive method, and this makes it attractive for the analysis of many important and complex samples and elements. As for using the SPA-L method, the number of metals obtained from the examined alloy were all foremost, petty, and impure metals.

Table 5. The minerals detected in the sample using both SPA-L and XRF techniques

SPA-L - Method								XRF- Technique	
Analytic Point	Con. %	A_P	Con. %	A_P	Con. %	A_P	Con. %	Symbol	Con. %
Ult. Al	97.629	Fe	1.358	Mn	0.0012	U	0.00035	Al	Remaining
Al	77.565	Si	0.472	Ni	0.068	Tm	0.0031	Fe	1.4
Al	70.386	Ti	0.028	V	0.048	Th	0.0028	Si	0.558
Al	58.812	Cr	0.089	Dy	0.0026	Zr	0.0023	Mg	0.042
Al	46.294	Co	0.078	Gd	0.0065	Pr	0.0012	-	
Al	21.129	Ca	0.098	Sm	0.0067	Ce	0.0025	-	
Al	12.333	Sc	0.004	P	0.0028	Nb	0.0016	-	
Al	9.859	Mg	0.039	Cl	0.0541	Etc.	-	-	
Al	7.655								
Al	7.651								
Low. Al	4.505								
99.999	Ult. 97.630		Σ = 2.1660		Σ = 0.1899		Σ = 0.0139		
	Foremost		**Petty**		**Impurity**		**Trace**		
Σ (Foremost+ Petty+ Impurity+ Trace) = 99.999									

ESTIMATE OF THE MECHANICAL PROPERTIES

In this paper, the tensile properties was conducted on the a high-purity Al alloy, addition to estimate the spectral properties of the unique spectral map points, that represent all foremost, petty and impure elements, each of these elements, in terms of quality and quantity, has an impact on the various properties of the selected aluminum alloy (X1, X2 and X3). Given that the alloy is exposed to mechanical and thermal stress due to high loads for transmitting electrical energy and ambient temperature (heating-cooling), which affects the properties and efficiency of this alloy as mechanical and electrical-conductivity properties.

These elements have varying amounts of influence on the mechanical properties depending on the quantity and quality of these metallic elements, as shown in Fig. 7. The tensile-properties behavior (Yield Strength YS, Ultimate tensile strength UTS),change in the YS and UTS is observed for each of the selected specimens of aluminum alloy. This is due to the difference in the proportion of the foremost and petty elements and impurities for each of the selected specimens, as shown in Table 6, which are difficult to determine quantitatively and qualitatively due to their low proportions and the sensitivity of these elements to other traditional test methods. This work highlights the tensile properties of a high-purity Al alloy, which are important properties of a high-purity Al alloy used in electrical

*Corresponding author
Bilal Ahmed Hbeeb,
Collage of production Engineering and metallurgical, University of Technology- Iraq, Baghdad, Iraq
e-mail: 70123@uotechnology.edu.iq

applications. However, there are other properties, such as electrical conductivity, and we suggest conducting a subsequent study to examine the effect of alloying elements on these properties.

Table 6. The concentrations of the foremost trace metals of reinforcement-iron classes

Class	% X_1	% X_2	% X_3
Foremost Element (Al)	97.629	96.242	98.105
Sum Petty Elements	2.166	3.096	1.612
Sum Impurity Elements	0.1899	0.5899	0.266
Sum Truce Elements	0.0139	0.0691	0.0163

The tensile test results at room temperature show slightly higher YS and UTS values when compared to the specified aluminum alloys (X1, X2, and X3). This is due to the difference in the proportions of alloying elements (major, minor, and impurities). These elements act as factors that hinder or prevent the movement of dislocations well.

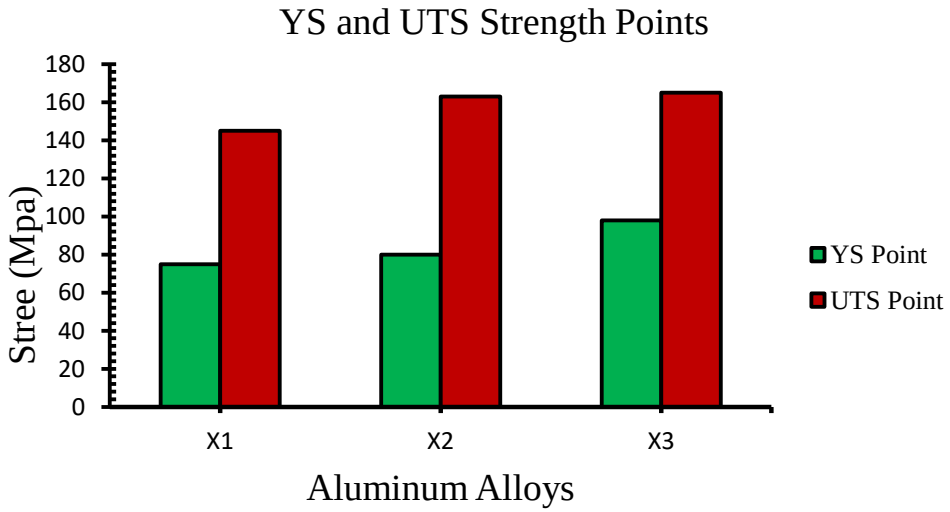

Fig. 7. The yield strength and ultimate tensile points of the selected aluminum alloys (X_1, X_2 and X_3) tested at ambient temperatures

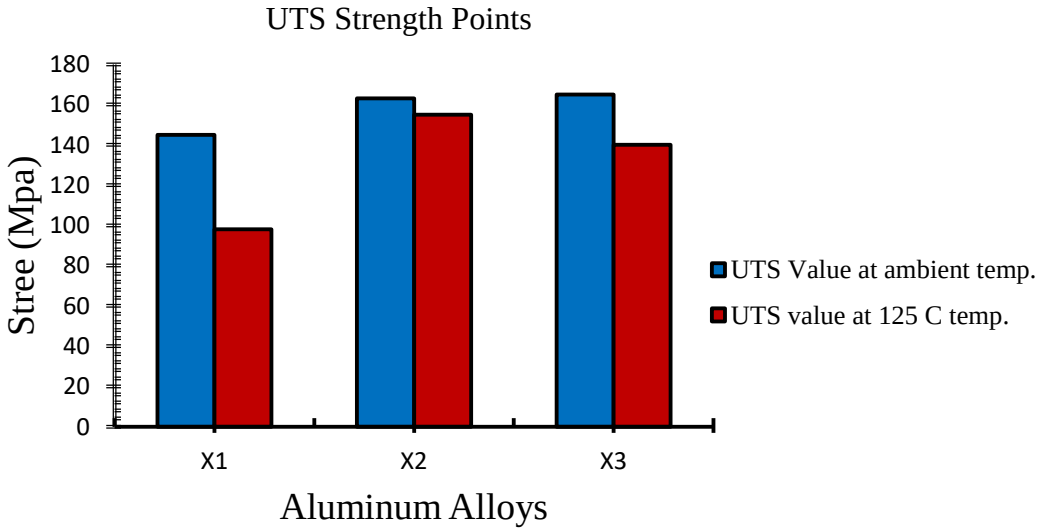

Fig. 8. The ultimate tensile strength values of the selected aluminum alloys (X_1, X_2, and X_3) tested at ambient and 125 °C temperatures

For the tested alloys at the elevated temperature (125°C), the YS and UTS values decreased or remained stable due to the easier movement of dislocations. as shown in Fig. 8. Compare the UTS values for alloys tested at ambient and 125°C temperatures. The results indicate a drop in UTS values at higher temperatures for the selected aluminum alloy

*Corresponding author
Bilal Ahmed Hbeeb,
Collage of production Engineering and metallurgical, University of Technology- Iraq, Baghdad, Iraq
e-mail: 70123@uotechnology.edu.iq

(X1, X2, and X3). This decrease is attributed to the easier movement of piled-up dislocations in the slip plane at 125°C.

This study can be used to collect results and information that can be exploited in the process of analyzing and evaluating problems, failures, and errors likely to occur in the future. In addition to reviewing and evaluating the efficiency and work of this alloy during work. Therefore, all these elements must be controlled by analyzing and capturing them accurately and correctly.

XRD ANALYSIS

Fig. 9 presents the X-ray diffraction (XRD) pattern of the a high-purity Al alloy, which corresponds closely to that of commercially pure aluminum, reflecting its very high aluminum content (typically above 99%). Structurally, these alloys crystallize in a cubic crystal system and adopt the face-centered cubic (FCC) crystal structure, also known as cubic close-packed (ccp). The structure belongs to the space group Fm-3m (No. 225) with a Pearson symbol cF4, indicating four atoms per cubic unit cell in a face-centered arrangement. The lattice parameter of aluminum at room temperature is approximately a = 4.05 Å, with commonly reported values ranging between 4.046 and 4.050 Å. Because a high-purity Al alloys contain only trace amounts of Fe, Si, and other elements, their fundamental diffraction behavior is essentially identical to that of pure aluminum, with negligible peak shifts or secondary reflections.

The characteristic XRD pattern of FCC aluminum contains a series of strong and well-defined reflections that correspond to the allowed (hkl) planes of the Fm-3m space group. Using Cu Kα radiation (λ = 1.5406 Å), the primary diffraction peaks appear at approximately 2θ = 38.5° for the (111) plane, 44.7° for the (200) plane, and 65.1° for the (220) plane. These are the three strongest reflections in the aluminum pattern, with the (111) peak being the most intense due to the high structure factor associated with its close-packed orientation. Additional higher-order peaks appear at 2θ ≈ 78.2° for the (311) plane and 82.4° for the (222) plane, both of which exhibit markedly lower intensity relative to the main reflections. The 2θ positions and relative intensities of these peaks follow the expected FCC relationship in which the quantity ($h^2+k^2+l^2$) determines the ordering of the reflections and ensures that only those peaks satisfying the FCC extinction rules are observed.

Peak positions in these alloys are generally consistent with the standard reference pattern for pure aluminum, most commonly represented by JCPDS/ICDD PDF Card No. 00-004-0787. This card is widely used to identify aluminum phases and provides a precise match for the XRD profile of a high-purity Al alloys materials. The excellent agreement between the measured peak positions and those listed in the PDF card confirms that the alloy exhibits a single-phase FCC aluminum matrix. Any variation in peak width or minor peak shifts relative to the reference may be attributed to factors such as grain refinement, residual strain, or the presence of extremely small quantities of Al–Fe–Si intermetallics, though these are typically undetectable or negligible in fully annealed a high-purity Al alloys.

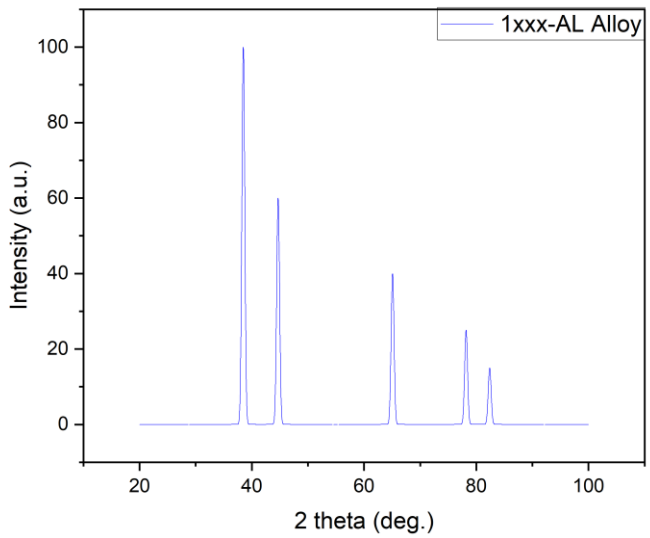

Fig. 9. X-ray diffraction pattern of the a high-purity Al alloys

*Corresponding author
Bilal Ahmed Hbeeb,
Collage of production Engineering and metallurgical, University of Technology- Iraq, Baghdad, Iraq
e-mail: 70123@uotechnology.edu.iq

AFM analysis

The 2D and 3D AFM images in Fig. 10 provide a nanoscale view of the surface topography of the sample, revealing how the surface height varies over the scanned area. The 2D image represents the height distribution as a color or grayscale map, where contrast corresponds to peaks and valleys, while the 3D image presents the same data as a three-dimensional landscape. Together, these visualizations allow you to qualitatively assess whether the surface is relatively smooth or rough, whether the asperities are uniformly distributed, and whether there are localized defects such as pits, grooves, or sharp protrusions. Even without strong directional features, AFM topography at this scale is very helpful for confirming that the surface preparation (e.g., polishing, etching, or coating) has produced a fairly homogeneous texture rather than a heavily damaged or uneven surface.

The roughness parameters you report, Sq = 50.44 nm and Sa = 40.87 nm, give a quantitative measure of that topography. Sa is the arithmetical mean height, representing the average absolute deviation of the surface heights from the mean plane over the scanned area. In simple terms, Sa ≈ 40.87 nm means that, on average, the surface profile deviates from a perfectly flat plane by a few tens of nanometers, indicating a nanoscale but measurable roughness. Sq is the root-mean-square (RMS) roughness, which weighs larger deviations more strongly than small ones. The value Sq = 50.44 nm being higher than Sa suggests that, in addition to the general background roughness, there are some asperities (either peaks or valleys) that are noticeably higher or deeper than the average, which increases the RMS value. This measurement is typical for surfaces where the height distribution is not perfectly uniform but still does not contain extremely large defects in the micrometer range.

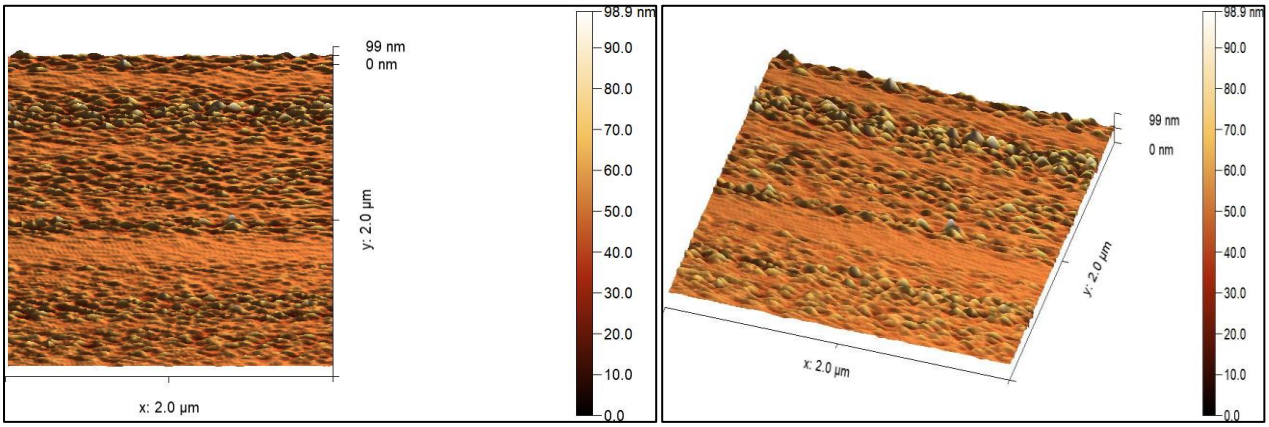

Fig. 10. AFM 2D and 3D images illustrating the nanoscale topography of the sample surface

ANTIBACTERIAL ACTIVITY

Fig. 11 reports the antibacterial assay results of square specimens against various microbial strains through ADM technique. Each Petri dish contains a square-shaped specimen resting on an inoculated agar surface (each isolated to replicate the bacterial species Staphylococcus faecalis (S.f2), Staphylococcus aureus (S.a2), Acinetobacter baumannii (AB2), Streptococcus citrus (S.c2) and Escherichia coli (Ec2)). The agar plates of all of the images demonstrate uniform bacterial growth up to the edges of the square samples, at no clear or measurable inhibitory regions around any of the specimens. The lack of observable halos would suggest that the active materials, if any, did not migrate significantly through the agar to inhibit bacteria growth. This indicates that the antibacterial effect for the samples is not likely to be true under diffusional-based conditions, or that it may require direct surface exposure as opposed to diffusion (which was not designed to be tested with ADM.) The uniformity of growth around each sample also supports the conclusion that there is no significant bactericidal or bacteriostatic effect for the materials in a diffusion based assay. Despite that, the ADM results merely show contact of the samples with bacterial cultures and it was no visual inhibition zone; therefore, additional antimicrobial tests, such as contact-kill, biofilm inhibition or time-kill studies may be necessary for a complete characterization of potential antimicrobial activity of all tested materials..

*Corresponding author
Bilal Ahmed Hbeeb,
Collage of production Engineering and metallurgical, University of Technology- Iraq, Baghdad, Iraq
e-mail: 70123@uotechnology.edu.iq

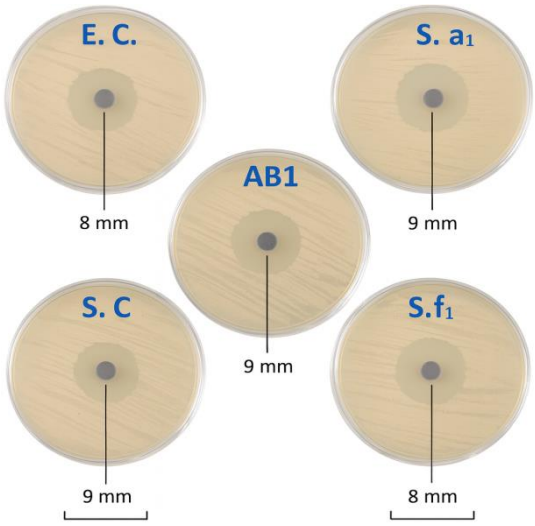

Fig. 11. Antibacterial activity of the tested material against five bacterial strains using the agar diffusion method

DISCUSSION

The test cluster, i.e., antibacterial activity, AFM experiment, XRD pattern results, and mechanical properties in addition to the yield strength and ultimate tensile points (YP and UTP) measurements illustrated in this work is a fine starting point for an understanding the properties of high-purity aluminum its alloys toward real applications. Each probes a different length scale or functional response, but all are linked together and to the relationship between alloy chemistry and microstructure with mechanical, surface and environmental behavior.

From practical perspective, anti-bacterial performance is more and more crucial for metals in a humid and dirty or biologically live surround such as outdoor infrastructures, housings or contacts which are the components involved in direct touch. Even though the agar diffusion test performed in this investigation did not show any inhibition zone above well diameter, this negative result should still be seen as informative: it illustrates that under conditions where diffusion plays a role, the favourable alloy and its surface state do not provide intrinsic antimicrobial protection. This highlights that, if antimicrobial activity is to be a feature of future designs, it ought not originate from the parent a high-purity Al alloy composition, but through specific and separate product features (such as coatings, nanoparticles or ions). It also demonstrates the relationship between surface chemistry, ion release and the potential for bio-interaction which is an increasingly important design dimension in multifunctional metallic systems..

In order to work on the surface with a resolution of nanomiters, AFM is combined with optical microscopy and enables quantitative topographical information. The roughness factors of 50.44 and 40.87 nm for □□ and □□ indicate that the nanoscale surface is moderately rough. Such roughness is important because it can influence several properties at the same time: contact mechanics and thus friction and wear features, effective surface area for electrochemical reactions with direct consequence on corrosion kinetics, also initial steps of staphylococcal adhesion and biofilm formation even if any antibacterial effect diffusive-based was observed. The potential benefits of a direct link between surface preparation, micro-damage at the micro-scale and functionally response via qualitative 3D images and quantitative roughness parameters are explored.

XRD analysis provides the phase-level picture and is crucial to ascertain that the material is a single-phase FCC Al matrix with minor intermetallics. This confirmation matters for a few reasons. One of them is that high-purity, single-phase FCC Al should have good electrical conductivity, which is the Achilles heel for power-transmission use. Second, the lack of strong secondary phases facilitates the interpretation of mechanical and corrosion behavior: deviations can be more easily ascribed to minor elemental additions or subtle microstructural alterations rather than bulk phase transformations. The good agreement with the DIN result and the lack of any other strong peaks make large-volume fractions (weak joints, more weak intermetallic) of brittle i-m possible which could decrease toughness, fatigue or local corrosion resistance.

The structural methods determine “what is there,” and mechanical properties tells you the local strength of response of the matrix and any near by phases. Mechanical test is especially sensitive to small changes in composition, dislocation density and precipitate content. As for high-purity aluminum, marginal changes of strengths are related with impurities and work hardening which also influence on its YS value as well as wear behavior. The tendency of strengths values between the Specimens (X1, X2, and X3) can be used to obtain an idea of how changing content petty and impurity element such as those that operate in strengthening or softening the alloy at the micro-level accordance with tensile test result.The effect of wear resistance is particularly important for components’ exposed in

*Corresponding author
Bilal Ahmed Hbeeb,
Collage of production Engineering and metallurgical, University of Technology- Iraq, Baghdad, Iraq
e-mail: 70123@uotechnology.edu.iq

sliding, fretting and mechanical contact such as connectors, clamps or mechanically loaded conductor regions. High-purity aluminum is soft by nature and susceptible to adhesive wear, so any enhancement of wear performance through controlled alloying or surface modification has potential application value. The wear tests link surface morphology (from AFM), local hardness (from strengths) and alloy chemistry (SPA-L/XRF) to material removal under simulated service conditions. A surface finish of intermediate roughness and hardness may have a lower wear rate than a very soft, mirror-bright finish which undergoes rapid plastic deformation and transfer.

PURE(99.9%)- AND HIGH-PURITY ALUMINUM While pure and high-purity aluminum are corrosion resistant because of the stable oxide film, the addition of minute quantities of Fe-, Si- or other elements may produce microgalvanic cells and localized attack. Thermocycling experiments thus act as a mechanical and spectral counterpart to corrosion tests: they determine whether the chemistry and microstructural observations via SPA-L, XRD, translate into long-term stability in the field. AFM and mechanical tests combined would also help to clarify whether corrosion starts from surface defects, inclusions or roughness features.

The integrated characterization toolbox based on antibacterial testing, chemistry and observations via SPA-L AFM, XRD, strengths along with YP and UTP measurements is well in line at the multi-scale level. It permits the alloy to be characterized not only in density and M 2 X mechanical properties, but also in surface integrity, wear resistance, and environmental interaction—important features for development and qualification of high-purity aluminum conductors for advanced systems.

CONCLUSION

Implications of the findings This study showed that plasma-based diagnostics can serve as an effective tool for microanalysis in high-purity Al alloys applied in engineering. Using the SPA-L method, was found an organized idea of aluminum plasma spectrum, which leads to a good recognition of lines analytical concentrations and assignment points, that form the Distinct Spectral Plasma Sign (DSPS). These spectroscopic signatures were critical for the determination of the temperature, density and elemental composition of the plasma with a sensitivity that cannot be obtained through ordinary XRF. The observation of petty, impurity and trace elements makes the development of SPA-L a tool for improvement in alloy assessment, in particular when minor constituents take effect on mechanical behavior or service performance.

Mechanical properties studies also proved that even slight changes in the chemical composition affect tensile strength, strain hardening and thermal stability. The tested samples displayed significant variations in yield and tensile strength among the three classes of alloys, with higher temperatures giving the anticipated softening behavior. Structural and topographical characterizations by XRD and AFM established the single-phase FCC Al matrix structure with a uniform nanoscale sized surface, in agreement with the mechanical results. The antibacterial tests showed that the alloys' surfaces did not provide any measurable inhibition on the strains tested, confirming that their composition and surface chemistry has been tailored more for electrical conductivity and mechanical strength than antimicrobial applications.

The results of the study demonstrate that SPA-L is a comprehensive, effective, and noninvasive tool that can be used to correlate plasma properties with alloy composition or performance. It can be used to enhance the quality assurance and future alloy design for electrical and structural applications.

REFERENCES

[1] Shahhosseininia, M., & Zamani, M. (2024). Deformation and strengthening behavior of Al-Cu-based alloys at ambient and elevated temperatures. Academia Materials Science, 1(4).

[2] Jayakumar, A., Radoor, S., Kim, J. T., Rhim, J. W., Parameswaranpillai, J., & Siengchin, S. (2023). Lightweight and sustainable materials—a global scenario. In Lightweight and Sustainable Composite Materials (pp. 1-18). Woodhead Publishing.

[3] Rana, R. S., Purohit, R., & Das, S. (2012). Reviews on the influences of alloying elements on the microstructure and mechanical properties of aluminum alloys and aluminum alloy composites. International Journal of Scientific and research publications, 2(6), 1-7.

[4] Yang, H., Sha, J., Zhao, D., He, F., Ma, Z., He, C., ... & Zhao, N. (2023). Defects control of aluminum alloys and their composites fabricated via laser powder bed fusion: A review. Journal of Materials Processing Technology, 319, 118064.

[5] George, E. T., & MacKenzie, D. S. (2003). Handbook of aluminum. Physical Metallurgy and Processes. New York: Marcel Dekker Inc.

[6] Caballero, F. G. (2021). Encyclopedia of materials: metals and alloys. (No Title).

[7] Kaufman, J. G., & Rooy, E. L. (2004). Aluminum alloy castings: properties, processes, and applications. Asm International.

*Corresponding author
Bilal Ahmed Hbeeb,
Collage of production Engineering and metallurgical, University of Technology- Iraq, Baghdad, Iraq
e-mail: 70123@uotechnology.edu.iq

[8] Shakiba, M., Parson, N., & Chen, X. G. (2015). Effect of iron and silicon content on the hot compressive deformation behavior of dilute Al-Fe-Si alloys. Journal of Materials Engineering and Performance, 24, 404-415.
[9] Davis, J. R. (1993). Aluminum and aluminum alloys. ASM international, p 59–87.
[10] Kaufman, J. G. (2000). Introduction to aluminum alloys and tempers. ASM international., p 87–118.
[11] McQueen, H. J., & Ryan, N. D. (2002). Constitutive analysis in hot working. Materials Science and Engineering: A, 322(1-2), 43-63.
[12] Mondol, S., Bansal, U., Dhanalakshmi, P., Makineni, S. K., Mandal, A., & Chattopadhyay, K. (2022). Enhancement of high temperature strength of Al-Cu alloys by minor alloying and hot working process. Journal of Alloys and Compounds, 921, 166136.
[13] Caballero, F. G. (2021). Encyclopedia of materials: metals and alloys. (No Title).
[14] Zhang, Y., Zhang, T., & Li, H. (2021). Application of laser-induced breakdown spectroscopy (LIBS) in environmental monitoring. Spectrochimica Acta Part B: Atomic Spectroscopy, 181, 106218.
[15] Hbeeb, B. A., Akbar, A. A., & Fawzi, A. K. (2022). Optimal Behavior of Spectral Line Analysis Through Fine Identification of Heavy Metal Lines in Crude Oil Using LIPS-Technique. In IOP Conference Series: Earth and Environmental Science (Vol. 961, No. 1, p. 012055). IOP Publishing.
[16] Mohannad H. Hussein , (2014) "Construction and operation of laser induced breakdown spectroscopy system for different material analysis" , M.Sc. Thesis , the University of Technology ; Bagdad, Iraq.
[17] Hbeeb, B. A., Akbar, A. A., & khaliq Fawzil, A. (2022, October). Quality assessment of heavy metals presented in crude oil by identification spectral lines by the LIPS-System. In 2022 International Symposium on Multidisciplinary Studies and Innovative Technologies (ISMSIT) (pp. 111-118). IEEE.
[18] Chen, T., Zhang, T., & Li, H. (2020). Applications of laser-induced breakdown spectroscopy (LIBS) combined with machine learning in geochemical and environmental resources exploration. TrAC Trends in Analytical Chemistry, 133, 116113.
[19] Kramida, A., Ralchenko, Y., & Reader, J. N. A. T. (2013, June). NIST atomic spectra database (version 5.1).
[20] Hbeeb, B. A., & Akbar, A. A. (2023, July). Evaluation of demetallization efficiency from crude oil by comparing laser-assisted with ultrasonic-assisted demetallization using lips-technology. In AIP Conference Proceedings (Vol. 2809, No. 1). AIP Publishing.
[21] Garcimuno, M., Pace, D. D., & Bertuccelli, G. (2013). Laser-induced breakdown spectroscopy for quantitative analysis of copper in algae. Optics & Laser Technology, 47, 26-30.
[22] Mohamed, W. T. Y. (2007). Study of the matrix effect on the plasma characterization of six elements in aluminum alloys using LIBS with a portable Echelle spectrometer. Progress in physics, 2, 42-49.
[23] Yamanouchi, K. (2015). Progress in Ultrafast Intense Laser Science VII. K. Yamanouchi, D. Charalambidis, & D. Normand (Eds.). Springer International Publishing.

*Corresponding author
Bilal Ahmed Hbeeb,
Collage of production Engineering and metallurgical, University of Technology- Iraq, Baghdad, Iraq
e-mail: 70123@uotechnology.edu.iq